Mon. Not. R. Astron. Soc. **000**, 000–000 (0000) Printed 22 July 2011 (MN LATEX style file v2.2)

The Non-linear Matter Power Spectrum in Warm Dark Matter Cosmologies

M. Viel[1,2], K. Markovič[3,4,5], M. Baldi[3,4], J. Weller[3,4,5]
[1] *INAF - Osservatorio Astronomico di Trieste, Via G.B. Tiepolo 11, I-34131 Trieste, Italy (viel@oats.inaf.it)*
[2] *INFN/National Institute for Nuclear Physics, Via Valerio 2, I-34127 Trieste, Italy*
[3] *University Observatory Munich, Ludwig-Maximilian University, Scheinerstr. 1, 81679, Munich, Germany*
[4] *Excellence Cluster Universe, Boltzmannstr. 2, 85748 Garching, Germany*
[5] *Max-Planck-Institut for Extraterrestrial Physics, Giessenbachstr., 85748 Garching, Germany*

22 July 2011

ABSTRACT
We investigate the non-linear evolution of the matter power spectrum by using a large set of high-resolution N-body/hydrodynamic simulations. The linear matter power in the initial conditions is consistently modified to accommodate warm dark matter particles which induce a small scale cut-off in the power as compared to standard cold dark matter scenarios. The impact of such thermal relics is addressed at small scales with $k > 1\,h\,\mathrm{Mpc}^{-1}$ and at $z < 5$, which are particularly important for the next generation of Lyman-α forest, weak lensing and galaxy clustering surveys. We quantify the mass and redshift dependence of the warm dark matter non-linear matter power and we provide a fitting formula which is accurate at the $\sim 2\%$ level below $z = 3$ and for masses $\mathrm{m_{WDM}} \geqslant 0.5$ keV. The role of baryonic physics (cooling, star formation and feedback recipes) on the warm dark matter induced suppression is also quantified. Furthermore, we compare our findings with the halo model and show their impact on the cosmic shear power spectra.

Key words: Cosmology: theory – large-scale structure of the Universe – dark matter, methods: numerical – gravitational lensing: weak

1 INTRODUCTION

The increasing amount of observational data available and the numerical tools developed for their interpretation have allowed to enter the so-called era of precision cosmology. At the present time, the concordance cosmological model based on a mixture of cold dark matter and a cosmological constant must thereby be tested in new regimes (both in space and in time) and using as many as possible observations and techniques in order to either confirm or disprove it.

Among the many different observables the non-linear matter power spectrum is a crucial ingredient since it allows to describe the clustering properties of matter at small scales and low-redshift, where linear theory is not reliable. However, non-linear physical processes that could affect this observable should be accurately modelled if quantitative results on the nature of dark matter are desidered.

Warm Dark Matter (WDM) is an intriguing possibility for a dark matter candidate whose velocity dispersion is intermediate between those of cold dark matter and hot dark matter (e.g. light neutrinos). In this scenario, at scales smaller than the free-streaming cosmological perturbations are erased and gravitational clustering is significantly suppressed. If such particles are initially in thermal equilibrium they have a smaller temperature and affect smaller scales than those affected by neutrinos, in addition WDM produces a distinctive suppression feature at such scales as compared to that induced by neutrinos. For example, thermal relics of masses at around 1 keV which constitute all of the dark matter have a free-streaming scale that is comparable to that of galaxies, well into the non-linear regime. Among the different warm dark matter candidates a special role is played by the sterile neutrino with mass in the keV scale (Boyarsky et al. (2009a)). Warm dark matter has been advocated originally to solve some putative problems that are present in cold dark matter scenarios at small scales (see Colín et al. (2000); Bode et al. (2001)), however it is at present controversial whether these tensions with cold dark matter predictions can be solved by modifying the nature of dark matter particles or by baryonic process (e.g. Trujillo-Gomez et al. (2010)).

In the present paper we wish to quantify the impact of a warm dark matter relic on the non-linear power spectrum by using a set of N-body/hydrodynamic simulations of cosmological volumes at high resolution. Investigating

WDM scenarios in a cosmological setting has been done by means of N-body codes in order to carefully quantify the impact of such a candidate in terms of halo mass function, structure formation, halo density properties (Bode et al. (2001); Colín et al. (2008); Colombi et al. (2009)) and particular care needs to be placed in addressing properly numerical/convergence issues Wang & White (2007). In general, while the WDM induced suppression transfer function can be reliably estimated in the linear regime (e.g. Viel et al. (2005); Lesgourgues & Tram (2011)), the non-linear suppression has not been investigated. A recent attempt to obtain the non-linear matter power at small scales by modifying the halo model has however been done in Smith & Markovic (2011).

The analysis of matter power spectra at small scales has been performed in recent years by different groups but focussing mainly on baryon physics (e.g. Rudd et al. (2008); Guillet et al. (2010); Casarini et al. (2011); van Daalen et al. (2011)) such as feedback and cooling) without considering how these properties are modified in WDM scenarios.

Different contraints can be obtained by using several astrophysical probes. For example by using SDSS Lyman-α observables such as the transmitted Lyman-α flux power very competitive constraints in the form of lower limits have been obtained (Viel et al. 2005, 2006; Seljak et al. 2006). The constraints are modified if the WDM is assumed to account only partially to dark matter (Boyarsky et al. 2009a) or if the initial linear suppression for a sterile neutrino is considered (Boyarsky et al. 2009b). Alternatively, constraints on WDM models can be placed by using the evolution and size of small scale structure in the local volume high resolution simulations (Tikhonov et al. 2009) the simulated Milky Way haloes to probe properties of satellite galaxies (Polisensky & Ricotti 2011; Lovell et al. 2011); large scale structure data (Abazajian 2006); the formation of the first stars and galaxies in high resolution simulations (Gao & Theuns 2007); weak lensing power spectra and cross-spectra (Markovic et al. 2011; Semboloni et al. 2011); the dynamics of the satellites (Knebe et al. 2008); the abundance of sub-structures (Colín et al. 2000); the inner properties of dwarf galaxies (Strigari et al. 2006); the mass function in the local group as determined from radio observations in HI (Zavala et al. 2009); the clustering properties of galaxies at small scales (Coil et al. 2008) and the properties of satellites as inferred from semi-analytical models of galaxy formation (Macciò & Fontanot 2010).

We believe that most of the astrophysical probes used so far in order to constrain the small scale properties of dark matter could benefit from a comprehensive numerical modeling of the non-linear matter power. The present work aims at providing such a quantity by using N-body/hydrodynamic simulations and the findings could also be useful for future surveys such as PanSTARRS (Kaiser et al. 2002), HETDEX (Hill et al. 2008), DES (Abbott et al. 2005), LSST (Ivezic et al. 2008), EUCLID (Refregier et al. 2010) or WFIRST[1].

The plan of the paper is as follows. In Section 2 we present our set of simulations and the code we use in order to investigate the non-linear suppression on the total matter power. Section 3 contains the main results of the present work and the description of the checks made in order to present a reliable estimate of the WDM non-linear suppression: we focus on numerical convergence, box-size, baryonic physics, particles' velocities and the effect induced by cosmological parameters on the WDM power. As an application of the findings of Section 3 we present in Section 4 the weak lensing power and cross-spectra for a realistic future weak lensing survey and compare these results with those that could be obtained by using either linear-theory or halo models (Section 5). We conclude with a summary in Section 6.

[1] http://wfirst.gsfc.nasa.gov/

linear size (Mpc/h)	m_{WDM}(keV)	soft. (kpc/h)
12.5	–	0.62
12.5	1	0.62
25^a	–	1.25
25	1	1.25
50	–	2.5
50	1	2.5
100	–	5
100	1	5
25	0.25	1.25
25	0.5	1.25
$25^{a,b,c}$	1	1.25
25	2	1.25
25	4	1.25
12.5	1	0.625
6.25	1	0.33

Table 1. Summary of the simulations performed. Linear box-size, mass of warm dark matter particle and gravitational softening are reported in comoving units (left, center and right columns, respectively). The particle-mesh (PM) grid is chosen to be equal to $N_{DM}^{1/3}$ with $N_{DM} = 512^3$. Simulations (a) have been run with hydrodynamic processes (a simplified star formation recipe and radiative processes for the gas) and with full hydrodynamics with the standard multiphase modelling of the interstellar medium and strong kinetic feedback in the form of galactic winds. Simulations (a) have been also run at lower resolution $N_{DM} = 384^3$ and for different values of σ_8 , Ω_m and H_0. Simulation (b) has been run by switching the initial velocities of warm dark matter particles off and by increasing the linear size of the PM grid by a factor 3. Simulation (c) has been run with $N_{DM} = 640^3$ dark matter particles with a softening of 1 kpc/h to $z = 0.5$.

2 THE SIMULATIONS

Our set of simulations has been run with the parallel hydrodynamic (TreeSPH: Tree-Smoothed Particle Hydrodynamics) code GADGET-2 based on the conservative 'entropy-formulation' of SPH (Springel 2005). Most of the runs use the TreePM (Tree-Particle Mesh) N-body set-up and consist only of dark matter particles, however for few runs, in order to test the impact of baryonic physics, we switched hydrodynamic processes on.

The cosmological reference model corresponds to a 'fiducial' ΛCDM Universe with parameters, at $z = 0$, $\Omega_m = 0.2711$, $\Omega_\Lambda = 0.7289$, $\Omega_b = 0.0451$, $n_s = 0.966$, and $H_0 = 70.3$ km s^{-1} Mpc^{-1} and $\sigma_8 = 0.809$. This model is in

agreement with the recent constraints obtained by WMAP-7 year data (Komatsu et al. 2011) and by other large scale structure probes. The initial (linear) power spectrum is generated at $z = 99$ with the public available software CAMB [2] (Lewis et al. 2000) and then modified to simulate warm dark matter (see below).

We consider different box sizes in order to both address the large scale power and (more importantly) the effect of resolution. The gravitational softening is set to be $1/40$-th of the mean linear inter-particle separation and is kept fixed in comoving units. The dimension of the PM grid, which is used for the long-range force computation, is chosen to be equal to the number of particles unless for a single case in which a finer grid is used. The simulations follow a cosmological periodic volume filled with 512^3 dark matter particles (an equal number of gas particles is used for the hydrodynamic simulations), unless for two cases in which a smaller and larger number of particles is chosen in order to check for numerical convergence of matter power. We mainly focus on warm dark matter masses around 1 keV. For such a mass, the characteristic cut-off in the power spectrum appears at scales of about $k \sim 1.5\ h\,\mathrm{Mpc}^{-1}$and reaches 50% at $k = 6\ h\,\mathrm{Mpc}^{-1}$: these scales are non-linear and thereby require high-resolution N-body techniques to be modeled. However, in order to be conservative we present results for the following $\mathrm{m_{WDM}}$values: 0.25, 0.5, 1, 2 and 4 keV. These limits could be easily converted to masses for a sterile neutrino particle produced in the so-called standard Dodelson-Widrow scenario (Dodelson & Widrow 1994) and corresponds to $m_\mathrm{s} = 0.7, 1.66, 4.4, 11.1, 28.1$ keV. Note that physically motivated scenarios for example based on non-resonant production mechanisms have been proposed, however the simulations carried in the present work cannot be strictly applied to those since they require a non-trivial modification of the linear transfer function, as discussed by Boyarsky et al. (2009b).

The initial conditions for warm dark matter particles are generated using the procedure described in Viel et al. (2005) and that we briefly summarize here. The linear ΛCDM power is multiplied by the following function:

$$T^2_\mathrm{lin}(k) \equiv P_\mathrm{WDM}(k)/P_\mathrm{\Lambda CDM}(k) = (1 + (\alpha\, k)^{2\nu})^{-5/\nu},$$
$$\alpha(\mathrm{m_{WDM}}) = 0.049 \left(\frac{1\mathrm{keV}}{\mathrm{m_{WDM}}}\right)^{1.11} \left(\frac{\Omega_\mathrm{WDM}}{0.25}\right)^{0.11} \left(\frac{h}{0.7}\right)^{1.22} \quad (1)$$

where $\nu = 1.12$ and α has units of h^{-1} Mpc (e.g. Hansen et al. 2002). We stress that the above equation is an approximation which is strictly valid only at $k < 5 - 10\ h\,\mathrm{Mpc}^{-1}$. Below this scale the warm dark matter power spectrum could be described by a more complicated function and acoustic oscillations are present (see for example the recent work in Lesgourgues & Tram 2011).

Initial velocities for warm dark matter particles are drawn from a Fermi-Dirac distribution and added to the proper velocity assigned by linear theory: the r.m.s. velocity dispersion associated to their thermal motion is 27.9, 11.5, 4.4. 1.7, 0.7 km/s for $\mathrm{m_{WDM}}$=0.25,0.5,1,2,4 keV, respectively. The typical r.m.s. velocity dispersion for the dark matter particles of the ΛCDM runs is ~ 27 km/s, so at least for masses above 1 keV the thermal WDM motion is a small fraction of the physical velocity dispersion assigned by the Zel'dovich approximation.

When baryonic physics is included we consider the following processes: *i*) radiative cooling and heating, *ii*) star formation processes, *iii*) feedback by galactic winds. The rationale is to see at which level these processes impact on the non-linear matter power at small scales in terms of warm dark matter suppression. Thus, we are not aiming at exploring in a comprehensive way the impact of these processes on the non-linear power at small scales. (e.g. van Daalen et al. 2011; Casarini et al. 2011): the baryonic simulations are used only to quantify the impact of such processes on the suppression induced by warm dark matter w.r.t. cold dark matter scenarios.

Radiative cooling and heating processes are followed for a primordial mix of hydrogen and helium by assuming a mean Ultraviolet Background similar to that produced by quasars and galaxies and implemented in Katz et al. (1996). This background gives naturally a hydrogen ionization rate $\Gamma_{12} \sim 1$ at high redshift and an evolution of the physical state of the intergalactic medium (IGM) which is in agreement with observations (e.g. Bolton et al. 2005). The star formation criterion for the default runs is a very simple one that converts in collisionless stars all the gas particles whose temperature falls below 10^5 K and whose density contrast is larger than 1000 (more details can be found in Viel et al. 2004). This prescription is usually called "QLYA" (quick Lyman-α) since it is very efficient in quantitatively describing the Lyman-α forest and the low density IGM. We also run a simulation with the full multi-phase description of the interstellar medium (ISM) and with kinetic feedback in the form of strong galactic winds as in Springel & Hernquist (2003). The chosen speed of the wind is 483 km/s and both the ISM modelling and this feedback mechanisms are expected to impact on the distribution of baryons and thus on the total matter power spectrum. We note that simulations that include baryons are significantly slower than the default (dark matter only runs) and therefore our constraints will be mainly derived by the former simulations.

In the following, the different simulations will be indicated by two numbers, (N_1, N_2): N_1 is the size of the box in comoving Mpc/h and N_2 is the cubic root of the total number of gas particles in the simulation. The mass per dark matter particle is $8.7 \times 10^6 \mathrm{M}_\odot/h$ for the default (25,512) simulations. This mass resolution allows to adequately sample the free-streaming mass for the models considered here.

In Figure 1 we show the projected dark matter density as extracted from the default (25,512) runs in the ΛCDM case (left) and WDM case (right) for $\mathrm{m_{WDM}}$=1 keV. This WDM particle mass is already ruled out at a significant level by Lyman-α forest observations (e.g. Seljak 2005; Viel et al. 2006). The different rows refer to $z = 0, 2, 5$ from top to bottom, respectively. In this Figure it is instrumental to see how the clustering proceeds differently in the two scenarios and while there are large differences below the Mpc scale at $z = 5$ between the two cosmic webs, these differences are largely erased by non-linear evolution at $z = 0, 2$.

The main features of the simulations are summarized in Table 1.

[2] http://camb.info/

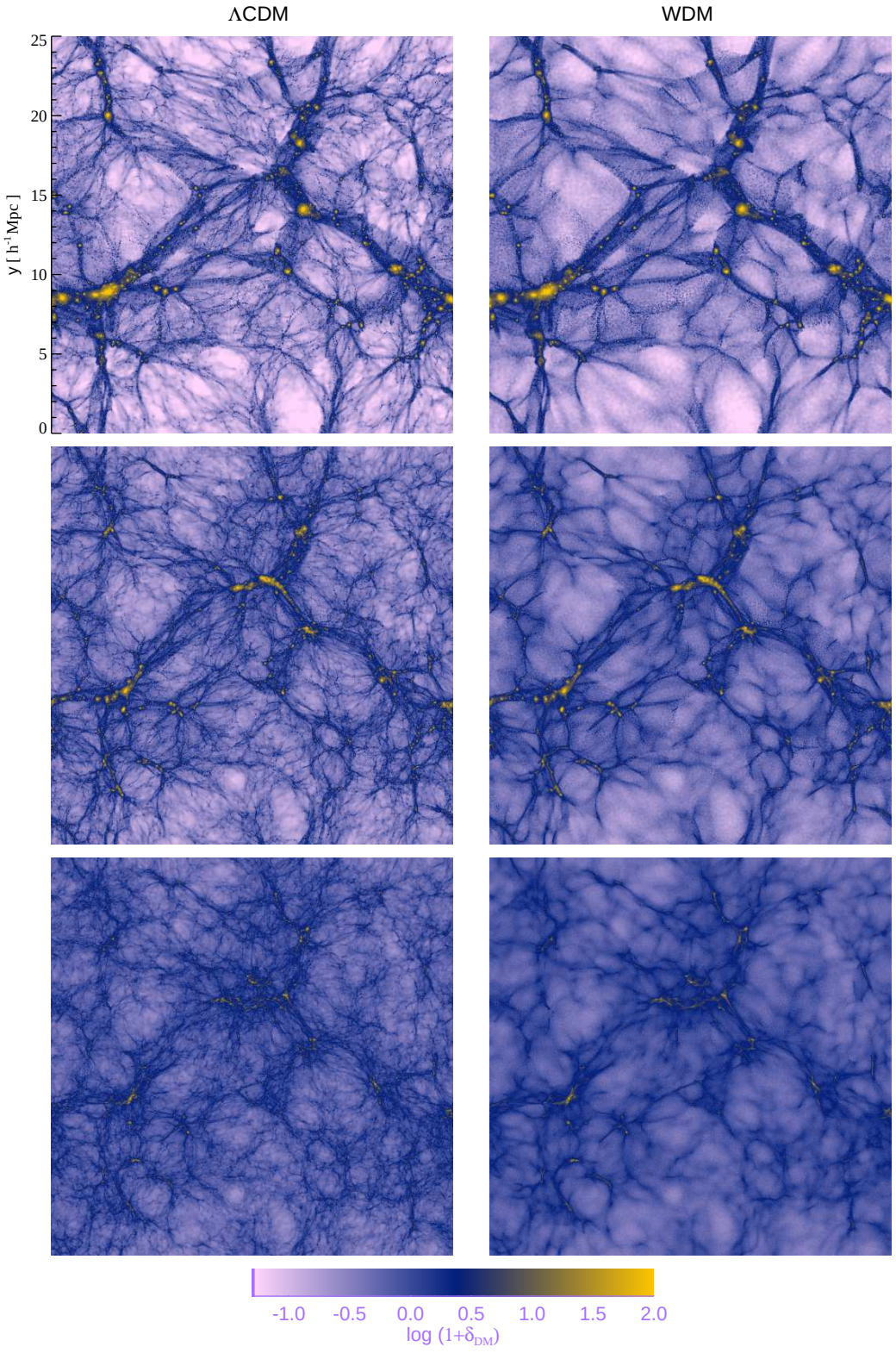

Figure 1. "Visual" inspection of the redshift evolution of cosmic structures in the ΛCDM and WDM ($m_{\rm WDM}$=1 keV) scenarios (left and right columns, respectively) for the defaults (25,512) runs. From the top to the bottom rows we show a 2.5 h^{-1} Mpcthick slice of the projected dark matter density at $z = 0$, 2 and 5 respectively. At $z = 0$ the clustering properties of the dark matter at scales $k < 10$ $h\,{\rm Mpc}^{-1}$are indistinguishable in the two scenarios, while at $z = 2, 5$ the WDM model has a suppression in power of about 5% and 25% at $k = 10$ $h\,{\rm Mpc}^{-1}$.

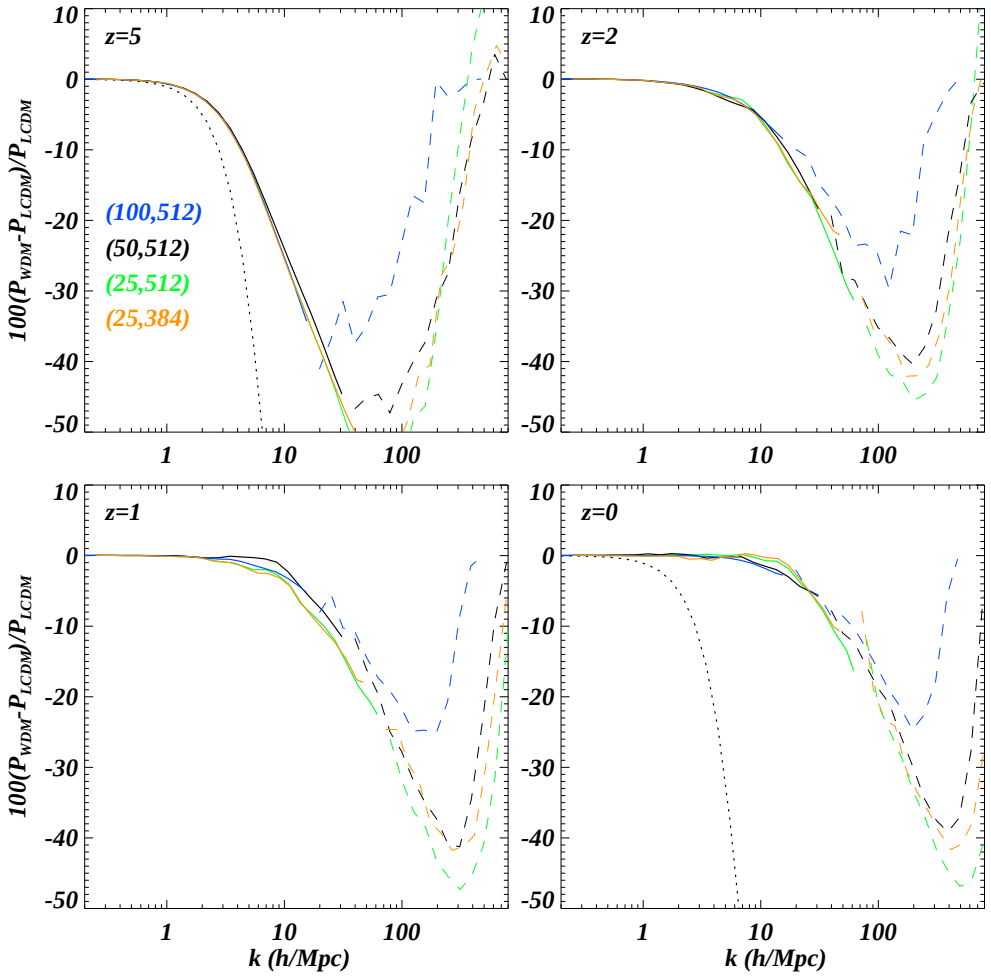

Figure 2. Percentage difference between warm dark matter non-linear power spectrum and cold dark matter for the different runs. The mass of the warm dark matter particle is kept fixed to $m_{WDM} = 1$ keV. Blue, black, green curves refer to 100, 50, 25 h^{-1} Mpcrespectively and with a fixed number of particles $N_{DM} = 512^3$. The orange curves refer to 25 h^{-1} Mpcand has a fixed number of particles $N_{DM} = 384^3$ The continuous lines represent the large scale estimate of the power, while the dashed ones describe the small scale power obtained with the folding method (see text). The four panels represent different redshifts at $z = 0, 1, 2, 5$ (bottom right, bottom left, top right and top left, respectively). The dotted line plotted at $z = 0$ and $z = 5$ is the redshift independent linear suppression between the two models.

3 RESULTS

In this Section we describe the main results obtained from our sample of simulations. The power spectrum is computed from the distribution of the different sets of particles (dark matter, gas and stars) separately and for the total matter component by performing a CIC (Cloud-In-Cell) assignment to a grid of the same size of the PM grid. The CIC kernel is also deconvolved when getting the density at the grid points (e.g. Viel et al. 2010)). We also show a small scale estimate ($k > 10\ h\,\mathrm{Mpc}^{-1}$) of the power spectrum obtained with the folding method described in (Jenkins et al. 1998; Colombi et al. 2009), although this power spectrum will not be used quantitatively.

We will plot the suppression in power spectrum as a percentage difference between WDM and ΛCDM matter power spectra, normalized by the default ΛCDM power spectrum. The initial conditions for CDM and WDM have the same phases and cosmological/astrophysical parameters in order to highlight the effect of the warm dark matter free streaming.

3.1 Resolution and box-size

In Figure 2 we show the percentage difference between the non-linear total power spectrum of WDM for m_{WDM}=1 keV and ΛCDM runs. We subtract the shot-noise from all the power spectrum estimates made. For our largest box-size simulations the shot-noise is comparable to the actual measured power spectrum at $z = 0$ at $k \sim 150\ h\,\mathrm{Mpc}^{-1}$, while for the default simulations (25,512) of m_{WDM}=1 (0.25) keV the matter power spectrum is always above the shot-noise level for $z < 10$ and for $k < 20(7)\ h\,\mathrm{Mpc}^{-1}$.

This figure focuses on the resolution and box-size effects

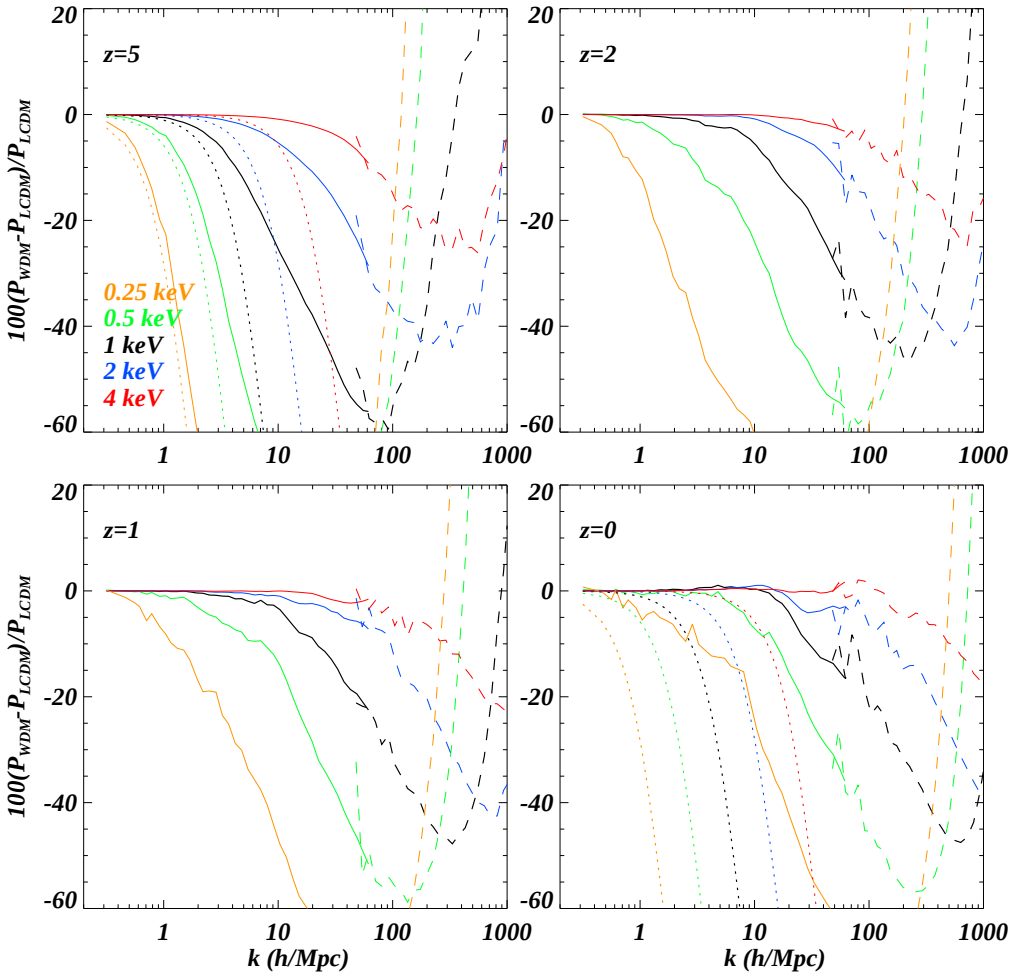

Figure 3. Percentage difference between warm dark matter non-linear power and cold dark matter for the different runs. The resolution is kept fixed in this plot and only 25 h^{-1} Mpcboxes are considered. Orange, green, black, blue and red curves refer to $\mathrm{m_{WDM}} = 0.25, 0.5, 1, 2, 4$ keV, respectively. The continuous lines represent the large scale estimate of the power, while the dashed ones describe the small scale power obtained with the folding method (see text). The four panels represent different redshifts at $z = 0, 1, 2, 5$ (bottom right, bottom left, top right and top left, respectively). The dotted coloured curves plotted at $z = 0$ and $z = 5$ are the redshift independent linear suppression between the different models.

and presents the ratio at four different redshifts $z = 0, 1, 3, 5$ (bottom right, bottom left, top right, top left panels, respectively) and for three different box-sizes (100, 50, 25 h^{-1} Mpc shown as blue, black and green curves). The dotted line represents the redshift independent linear cut-off of Eq.1, while the lower resolution (25,384) run is also plotted as orange curves. Here there are two estimates for the power spectrum: one at large scales (solid curves), the second at smaller scales (dashed curves). We are primarily interested in the power at scales $k < 10\ h\,\mathrm{Mpc}^{-1}$and thereby only the large scale estimate will be used, however, we decide also to show the power at smaller scales since physical and numerical effects play a larger role in this range. We note that the linear theory suppression is a good approximation only at $k < 1\ h\,\mathrm{Mpc}^{-1}$. From Figure 2 one can see that there is convergence up to $k = 50\ h\,\mathrm{Mpc}^{-1}$between (25,512) and (25,384) runs in all the redshift range considered. The resolution used is thus sufficient for $\mathrm{m_{WDM}}$=1 keV particles. Note that van Daalen et al. (2011) have recently found that (100,512) ΛCDM simulations have sufficiently converged at scales $k < 10\ h\,\mathrm{Mpc}^{-1}$. At $k = 3(10)\ h^{-1}\,\mathrm{Mpc}$ and $z = 5$ there is already a 5 (50)% difference between the linear and non-linear power. At $z = 0, 1, 3$ the differences between WDM and ΛCDM power is 1,3 and 5% respectively at $k = 10\ h\,\mathrm{Mpc}^{-1}$. The maximum suppression dip is strongly influenced by resolution and moves to larger wavenumbers when the resolution increases. At $k > 100\ h\,\mathrm{Mpc}^{-1}$we note a steep (resolution dependent) turn-over in the suppression which is likely to be due to effects that impact on the halo structure and which has also been found in numerical simulations that include a fraction of the matter content in the form of active neutrinos (Brandbyge et al. 2008; Viel et al. 2010).

We have checked that increasing the particle-mesh grid

by a factor three (i.e. PM=1536) has negligible impact on the total matter power at scales $k < 100\ h\,\mathrm{Mpc}^{-1}$. In order to test the robustness of our results in terms of shot-noise level we have also run a WDM simulation with $\mathrm{m_{WDM}}$=1 keV and $N_{\rm DM} = 640^3$ particles and compared the power spectra with the (25,512) and (25,384) runs: we confirm very good agreement between these simulations at $k < 20\ h\,\mathrm{Mpc}^{-1}$in the redshift range considered in the present work. More precisely, the (25,512) and (25,640) WDM runs agree below the one percent level at $k < 100\ h\,\mathrm{Mpc}^{-1}$.

3.2 The effect of the mass of a warm dark matter particle

Here we address the effect of a different value of $\mathrm{m_{WDM}}$ on the non-linear matter power spectrum. The results are shown in Figure 3 where we report five different masses for the (25,512) default runs. The masses refer to $\mathrm{m_{WDM}}$=0.25,0.5,1,2 and 4 keV (orange, green, black, blue and red curves, respectively) at $z = 0, 1, 2$ and 5 (bottom right, bottom left, top right and top left, respectively). The linear suppressions are also shown with dotted lines of the corresponding colors. At $z = 5$ we can see large differences between the models that become smaller with the redshift evolution. The 20% suppression at $k = 10\ h\,\mathrm{Mpc}^{-1}$for the $\mathrm{m_{WDM}}$=1 keV model becomes 2% at $z = 1$ and disappears at $z = 0$. Basically the clustering properties of the dark matter are the same at scales above $k \sim 10\ h\,\mathrm{Mpc}^{-1}$at least for $\mathrm{m_{WDM}}$> 1 keV. The $\mathrm{m_{WDM}}$=0.5 keV model still presents a 7% suppression by $z = 0$, while the suppression is four times larger at $z = 2$. The linear suppression is a very poor approximation in the range of wavenumbers considered here even at high redshift. At $z = 1$, which is particularly interesting for weak lensing data, a 2% measurement of the non-linear power is likely to be able to exclude models below the 1 keV value (bottom left panel). The dip of maximum suppression and the turn-over both move to larger scales as the mass decreases.

We have also investigated the importance of the warm dark matter velocities in the initial conditions by running a simulation without adding the Fermi-Dirac drawn thermal velocity to the dark matter particles. We tested this for a $\mathrm{m_{WDM}}$=1 keV model and found differences always below 1% in terms of total matter power spectrum at the scales of interest here.

3.3 Baryonic effects

In this section we explore the effects of baryonic physics on the warm dark matter suppression. Baryons amount to about 17% of the total matter content and we expect that astrophysical processes affecting their properties can impact on the total matter distribution at small scales. We identify three effects that are able to modify the clustering properties of baryons: radiative processes, star formation and galactic feedback. These processes are usually modelled by hydrodynamic simulations of galaxy formation. Here, the main goal is not to explore fully the many parameters governing these important physical aspects, but rather to address their impact in warm dark matter models by adopting prescriptions that are widely used in the literature. There could well be other astrophysical processes (radiative transfer effects, feedback from active galactic nuclei, etc.) that can also affect the distribution of baryons and their clustering properties (see for example van Daalen et al. 2011).

In Figure 4 we plot the warm dark matter suppression for the default simulation of $\mathrm{m_{WDM}}$=1 keV for three different cases: pure dark matter (green curves); a hydrodynamic simulation that include cooling and heating by an ultraviolet background and the simple star formation criterion able to simulate the Lyman-α forest ("BARYONS+QLYA" run in blue); a hydrodynamic simulation that does include the full (sophisticated compared to QLYA implementation described above) star formation model based on the multi-phase description of the ISM (Springel & Hernquist 2003) and strong galactic feedback in the form of winds ("BARYONS+SF+WINDS" in black). Unfortunately, due to the fact that hydrodynamic simulations are slower than dark matter only runs it was not possible to carry the this last simulation down to $z = 0$ and it was stopped at $z = 1.2$.

All of these processes can significantly change the clustering of baryons especially at intermediate scales where baryon pressure is important ($k \sim 1\ h\,\mathrm{Mpc}^{-1}$), and where they are not expected to trace the dark matter, and at smaller scales given the complex interplay between feedback and star formation processes. Cooling and heating modify the thermal properties of the gas and are important especially for the low density IGM; the star formation criterion determines how much gas is turned into stars within the potential wells of dark matter haloes; galactic winds displace gas out of the galaxies into the low density IGM and usually in a hot phase that prevents subsequent cooling. Since the cosmic structure is different between CDM and WDM models in general we do not expect the warm dark matter suppression to be exactly the same between two simulations that share the same astrophysical prescriptions. From Figure 4, one can see that the dark matter only simulations and the one with radiative cooling and QLYA star formation are in good agreement at the percent level up to $k = 10\ h\,\mathrm{Mpc}^{-1}$, while at smaller scales there are significant differences and it is clear that the presence of baryons and star formation greatly affects the maximum suppression and the turn-over. Note that differences much larger than 10% between simulations implementing different radiative processes (e.g. metal cooling) or feedback recipes are expected at $k > 20\ h\,\mathrm{Mpc}^{-1}$in ΛCDM models (see e.g. Rudd et al. 2008; Guillet et al. 2010; van Daalen et al. 2011). In the $z = 0$ panel we also show the difference in the power spectra of ΛCDM and WDM models by normalizing to the corresponding dark matter only model: in such a way we highlight the effect of cooling produced by the baryons and not the WDM signature. The two percentage differences are shown as cyan (WDM) and red (ΛCDM) curves: the WDM universe when filled with baryons that can cool has more power than a corresponding ΛCDM universe filled with the same baryon fraction. The quantity $P_{\rm nl,WDM,cooling}/P_{\rm nl,WDM,dmonly}$ is about 5% larger than $P_{\rm nl,\Lambda CDM,cooling}/P_{\rm nl,\Lambda CDM,dmonly}$ at $k = 10\ h\,\mathrm{Mpc}^{-1}$and $z = 5$, becomes only 2 % larger at $z = 1$, and by $z = 0$ there are no differences at the same wavenumber between the two quantities. The cooling of baryons inside the potential wells of dark matter haloes produces further collapse of structures and in general increases the (total) matter power spectrum. It is thus likely that in the WDM model

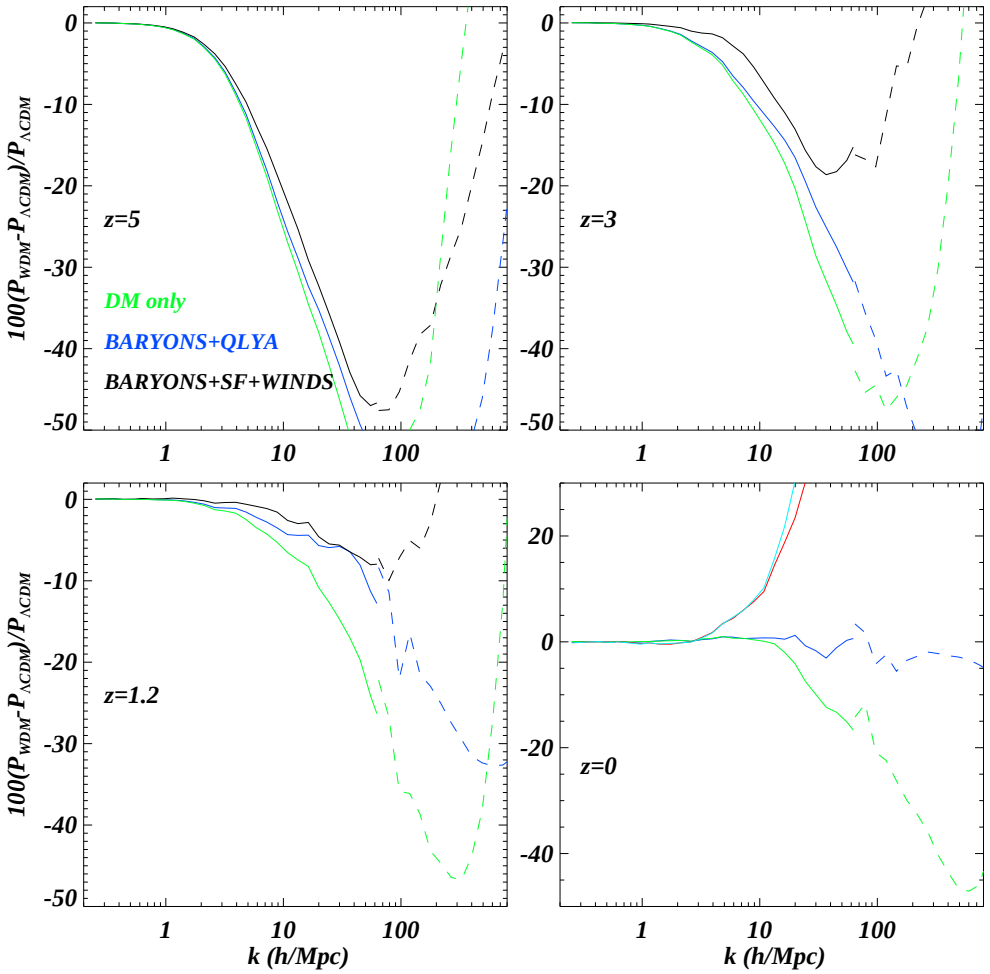

Figure 4. Percentage difference between warm dark matter non-linear power and cold dark matter for different runs that incorporate baryonic physical processes. The simulations refer to a 25 h^{-1} Mpcbox and $m_{\rm WDM}$=1 keV. The green curves refer to the pure dark matter simulations; blue curves refer to simulations that include baryons, cooling and a simplified recipe for star formation that turns into collisionless stars all the gas particle below T=10^5 K and denser than 1000 times the mean density (QLYA); black curves are instead obtained by using the default criterion of multi-phase star formation of Springel (2005) and feedback in the form of strong kinetic driven winds (this simulation was stopped at $z = 1.2$). The continuous lines represent the large scale estimate of the power, while the dashed ones describe the small scale power obtained with the folding method (see text). The four panels represent different redshifts at $z = 0, 1.2, 3, 5$ (bottom right, bottom left, top right and top left, respectively). In the $z = 0$ panel (note the different scale for the $y-$axis) we also show as the red and cyan curves the percentage of the matter power spectra that include and do not include cooling for ΛCDM (red) and WDM (cyan) models, respectively (i.e. $100 \times (P_{\rm mat}^{\rm baryons+QLYA} - P_{\rm mat}^{\rm DMONLY})/P_{\rm mat}^{\rm DMONLY}$).

the baryons cool slightly more efficiently than in the corresponding ΛCDM since at high redshift the collapse of haloes around the WDM cutoff is rapid and small scale modes affected by cooling grow more rapidly than in CDM: this is also the trend found by Gao & Theuns (2007) from the analysis of cooling at very high resolution and high redshift in hydrodynamic simulations.

The warm dark matter suppression is thereby highly influenced by astrophysics effects at $k = 100\ h\,{\rm Mpc}^{-1}$and in general we expect a a suppression of about 2-3% at $k = 10\ h\,{\rm Mpc}^{-1}$and at $z > 1.5$ for the $m_{\rm WDM}$=1 keV case once baryons are included, while this discrepancy becomes smaller at lower redshifts.

To sum up, any attempt to recover the total non linear matter power at $z < 5$ and at scales $k = 1 - 10\ h\,{\rm Mpc}^{-1}$should heavily rely on a proper modelling of astrophysical aspects such as radiative processes, feedback and star formation recipes.

3.4 Other cosmological parameters

To test the robustness of our results we extended the set of simulations by exploring also other cosmological parameters, namely: $\Omega_{\rm m}$, H_0 and σ_8. In order to do that we modified the input linear ΛCDM parameter calculated by CAMB and vary one parameter at a time. Some parameters, such as σ_8 (or

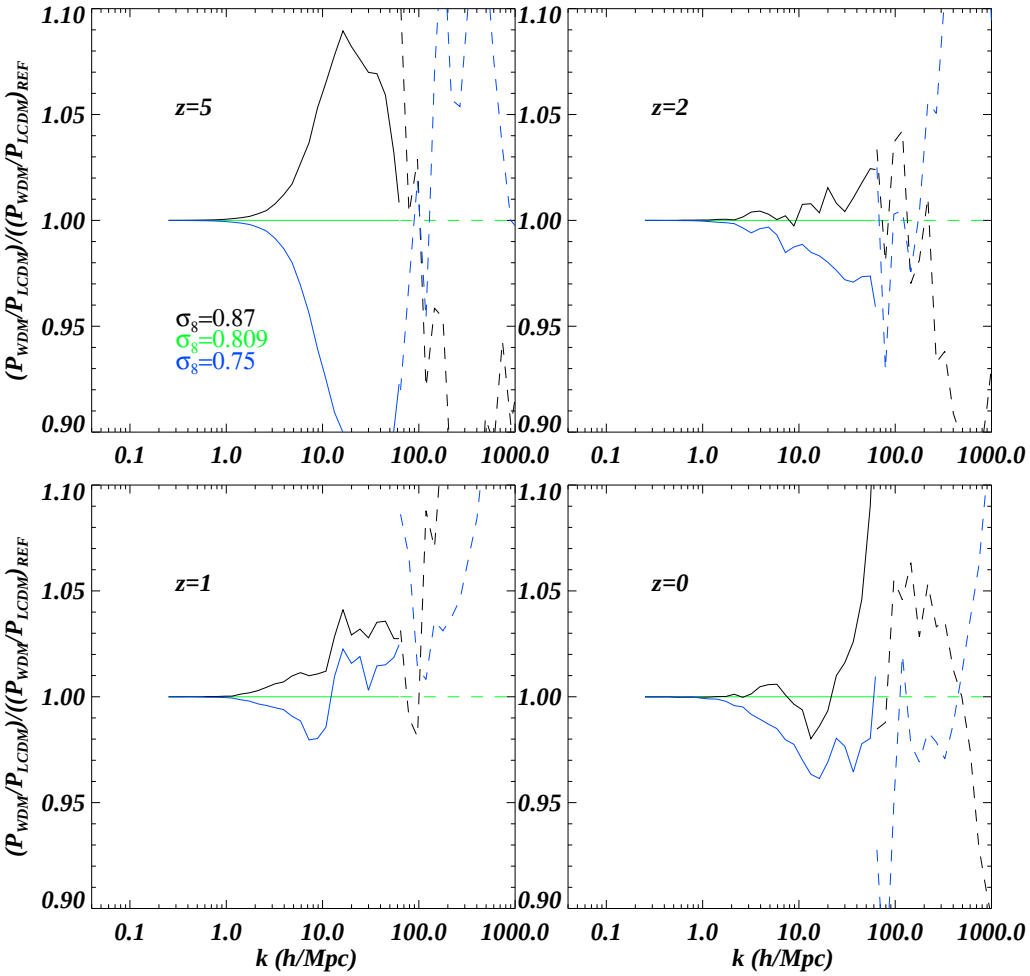

Figure 5. Impact of a different σ_8 value in terms of WDM-induced suppression. The four panels represent different redshifts at $z = 0, 1, 2, 5$ (bottom right, bottom left, top right and top left, respectively) for the (25,512) with $m_{\rm WDM}$=1 keV. Green represents the ($\sigma_8 = 0.809$) reference case, while the two other curves indicate the suppression for $\sigma_8 = 0.87$ (black) and $\sigma_8 = 0.75$ (blue).

A_s), only boost the amplitude of the power spectrum but do not change the shape. However the boost of power can have also effects on the non-linear level. We choose the following parameters for the WDM and corresponding ΛCDM runs: $\Omega_{\rm m} = 0.22, 0.32$, $H_0 = 62, 78$ km/s/Mpc and $\sigma_8 = 0.75, 0.87$. When calculating the suppression we always normalize both the simulations to the same σ_8 value ($\sigma_8 = 0.75, 0.809$ and 0.87). Since the WDM cut-off, for the WDM models investigated here, appears at much smaller scales than those probed by the σ_8 normalization, this requirement, together with the fact that the WDM suppression has a very distinctive feature, will make the suppression nearly independent from any other parameter probed. The range explored by the H_0 values produces a maximum ±2% difference in terms of the WDM suppression compared to the reference $H_0 = 70.3$ km/s/Mpc case at $k = 1 - 10\ h\,{\rm Mpc}^{-1}$and at $z < 3$, while at $z = 5$ there is a 5% difference at $k = 10\ h\,{\rm Mpc}^{-1}$. The $\Omega_{\rm m}$ parameter produces a maximum difference of 1% at $z < 3$ in the same range of wavenumbers and about 5% at $z = 5$ and $k = 10\ h\,{\rm Mpc}^{-1}$. A slightly larger impact is the one induced by a different choice of σ_8 that we show in Figure 5 where the WDM induced suppression is divided by the reference case: it is clear that the large (10 %) differences in place at $z = 5$ are largely canceled by the non-linear growth and are at the ±2% level at $z = 1 - 2$ and at the 3% level at $k = 10\ h\,{\rm Mpc}^{-1}$and $z = 0$.

Motivated by the present findings we regard our non-linear cutoff and its redshift dependence as robust at least for the range of cosmological parameters investigated at $z < 3$, for $m_{\rm WDM} \geqslant 0.5$ keV and at $k = 1 - 10\ h\,{\rm Mpc}^{-1}$: in fact the differences are at the ± 2% level and in the next section we will provide a fitting formula with a comparable level of accuracy. Larger masses for $m_{\rm WDM}$ will only result in smaller differences in terms of WDM suppression.

We also notice that degenerate features with the non-linear WDM suppression might arise in the context of non-standard models of dark energy, as e.g. interacting dark energy scenarios (see e.g. Baldi 2011). The investigation of such possible degeneracies goes beyond the scope of the present paper.

3.5 An analytical fitting formula

Inspired by the corresponding formula for the linear suppression, we have found the following fitting formula to be a good approximation of the late time evolution of the non-linear suppression with an accuracy at the 2% level at $z < 3$ and for masses larger than $\mathrm{m_{WDM}}$=0.5 keV:

$$T^2_{\rm nl}(k) \equiv P_{\rm WDM}(k)/P_{\Lambda{\rm CDM}}(k) = (1+(\alpha\, k)^{\nu l})^{-s/\nu},$$
$$\alpha(\mathrm{m_{WDM}}, z) = 0.0476 \left(\frac{1\mathrm{keV}}{\mathrm{m_{WDM}}}\right)^{1.85} \left(\frac{1+z}{2}\right)^{1.3}, \quad (2)$$

with $\nu = 3$, $l = 0.6$ and $s = 0.4$.

We have chosen as a pivot redshift $z = 1$ since this is the redshift where accurate weak lensing data will be available. The accuracy of this fitting procedure is discussed below and shown in Figure 7.

4 WEAK LENSING SHEAR POWER SPECTRA

Following Markovic et al. (2011) and Smith & Markovic (2011), we examine the effect of the fitting function in Equation 2 on the weak lensing power spectrum. Weak gravitational lensing is the distortion found in images of distant galaxies due to the deflection of light from these galaxies by the gravitational potential wells of intervening matter. For a review, see for example Bartelmann & Schneider (2001). The advantage of gravitational lensing is that unlike other Large Scale Structure data, it does not require a knowledge of galaxy bias for the derivation of the properties of the underlying dark matter density field and is, at least on large scales, independent of baryonic physics. In other words, the weak lensing power spectrum directly probes the matter power spectrum. However, weak lensing measures the matter power spectrum at low redshifts. For this reason it is necessary to have available robust models of non-linear structure. For a survey able to probe angular multipoles from $l \sim 20$ up to $l \sim 2\times10^4$, in the redshift range of $z = 0.5-2.0$, the corresponding range of wavenumbers must be $k \sim 0.005 - 15\ h\,\mathrm{Mpc}^{-1}$. Note that the matter power at $k > 10\ h\,\mathrm{Mpc}^{-1}$only has a significant contribution to the weak lensing power spectrum at lower redshifts, where however the lensing power is lower.

Future weak lensing surveys accompanied by extensive photometric redshift surveys will be able to disentangle the contribution to weak lensing by dark matter at different redshifts, by binning source galaxies into tomographic bins (Hu 1999). By cross and auto correlations of the lensing power in these bins, the three dimensional dark matter distribution can be reconstructed. An existing example of such a reconstruction is the COSMOS field (Massey et al. 2007). Such tomography probes the non-linear matter power spectrum at different redshifts.

We use HALOFIT (Smith et al. 2003) to calculate non-linear corrections to the approximate linear matter power spectrum (Ma 1996). We then apply Equation 2 to approximate the WDM effects and find the weak lensing power spectrum (e.g. Takada & Jain 2004):

$$C_{ij}(l) = \int_0^{\chi_{\rm H}} d\chi_{\rm l} W_i(\chi_{\rm l}) W_j(\chi_{\rm l}) \chi_{\rm l}^{-2} P_{\rm nl}\left(k=\frac{l}{\chi_{\rm l}}, \chi_{\rm l}\right), \quad (3)$$

where $\chi_{\rm l}(z_{\rm l})$ is the comoving distance to the lens at redshift $z_{\rm l}$ and W_i is the lensing weight in the tomographic bin i:

$$W_i(z_{\rm l}) = \frac{4\pi G}{a_{\rm l}(z_{\rm l})c^2}\rho_{\rm m,0}\chi_{\rm l}\int_{z_{\rm l}}^{z_{\rm max}} n_i(z_{\rm s})\frac{\chi_{\rm ls}(z_{\rm s}, z_{\rm l})}{\chi_{\rm s}(z_{\rm s})}dz_{\rm s} \quad , \quad (4)$$

where we assume a flat universe and $a_{\rm l}(z_{\rm l})$ is the scale factor at the redshift of the lens, $\rho_{\rm m,0}$ is the matter energy density today and $n_i(z_{\rm s})$ is the normalised redshift distribution of sources in the i-th tomographic bin. We bin the multipoles into 20 bins.

In order to asses detectability of WDM by future weak lensing surveys, we calculate predicted error bars on the weak lensing power spectrum using the covariance matrix formalism (Takada & Jain 2004) and assuming errors for a future realistic Weak Lensing survey as in Markovic et al. (2011) and Smith & Markovic (2011) with 8 redshift bins in the range $z = 0.5 - 2.0$. We plot the resulting percentage differences between WDM and CDM weak lensing power spectra in figure 6. It is important to note that the error bars in the figure do not fully characterise the sensitivity of the power spectra, since there are additional correlations between the error bars of different bin combinations. Additionally, there are correlations in the error bars on large l (small scales) due to non-linearities. Further statistical tests using the entire covariance matrix must be used in order to fully account for the above correlations. For this plot we choose only the $5-th$ and $8-th$ redshift bins, whose source galaxy distributions have the mean at $z \sim 1.0$ and 1.6 respectively. These bins are chosen because they represent a range with the maximal WDM effect as well as lensing signal. Note that the upturn around $l \sim 10^3$ in the auto-correlation power spectra of bins 5 and 8 is due to the dominance of shot noise on those scales. This noise is due to intrinsic galaxy ellipticities and can be eliminated by cross-correlating different redshift bins, as can also be seen in Figure 6 (see also Takada & Jain 2004).

In the right panel of Figure 6 we plot the effects of the 0.5 keV particle and since the black dashed line lies far outside the error bars this is a strong indication that such a particle can be ruled out (or detected) by a future weak lensing survey. This is consistent with previous works (Markovic et al. 2011; Smith & Markovic 2011). In the left panel of Figure 6 we plot the effects of a 1 keV WDM particle: in this case it is more difficult to distinguish from CDM (black dashed line), but the strongly affected cross power spectra are still significantly different from their expected values in ΛCDM.

5 COMPARISON WITH HALO MODEL

As described in Section 4, it is necessary to have a robust model of non-linear structure in order to take full advantage of future weak lensing data. For this reason we compare the non-linear matter power spectra extracted from the simulations with previously derived non-linear models. The halo model of non-linear structure is based on the assumption that large scale structure is made up of individual objects occupying peaks in the matter overdensity field (Press & Schechter 1974; Seljak 2000; Cooray & Sheth 2002). The most important elements of this model, the mass function, the halo bias (Press & Schechter 1974) and the

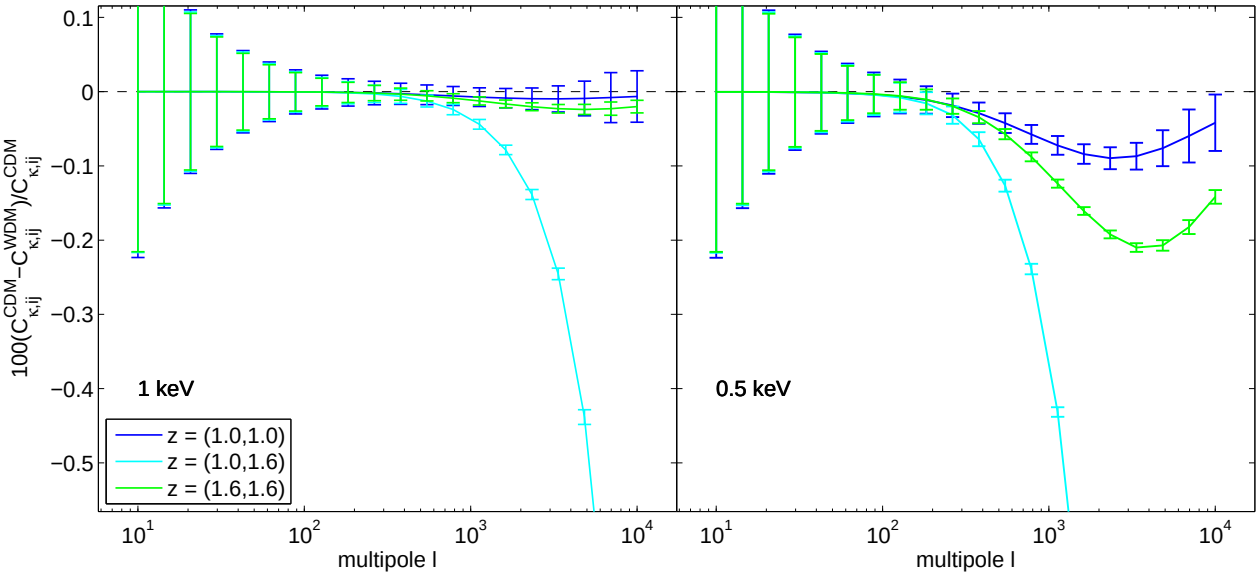

Figure 6. The percentage WDM effect in auto- and cross-correlation power spectra of redshift bins at approximately $z = 1$ and $z = 1.6$, respectively. All the lines are calculated from non-linear matter power spectra modified for WDM by the fitting function in Equation 2 for WDM particle masses of 1 keV (left panel) and 0.5 keV (right panel). In addition we plot predicted error bars for a future weak lensing survey, dividing the multipoles into 20 redshift bins. Note that the error bars on auto and cross power spectra of different bins are correlated and therefore in order to fully characterise the detectable differences between the WDM (solid lines) and CDM (dashed black line at 0) models, one must know the entire covariance matrix for a survey. Note secondly that the auto power spectra of redshift bins at $z = 1$ and $z = 1.6$ have an upturn around $l \sim 10^3$. This is due to the dominance of shot noise on those scales. This upturn is not present in the cross power spectrum, because through cross correlation this noise due to intrinsic galaxy ellipticities is eliminated.

halo density profile (Navarro et al. 1995) are based on the assumptions that all dark matter in the universe is found in haloes and that there is no observable suppression of small scale overdensities from early-times free-streaming of dark matter particles or late-times thermal velocities.

These are characteristic properties of CDM, but do not apply to WDM. For this reason Smith & Markovic (2011) modified the halo model by applying a specific prescription to the non-linear contribution, in addition to suppressing the initial density field, modelled by applying a transfer function from Viel et al. (2005) to the linear matter power spectrum. Such prescription consists in: *i*) treating the dark matter density field as made up of two components: a smooth, linear component and a non-linear component, both with power at all scales; *ii*) introducing a cut-off mass scale, below which no haloes are found; *iii*) suppressing the mass function also above the cut-off scale and *iv*) suppressing the centres of halo density profiles by convolving them with a Gaussian function, whose width depended on the WDM relic thermal velocity.

Here, we do not attempt to explore each of these elements with simulations individually, but rather compare the final matter power spectra found from simulations and from the WDM halo model of Smith & Markovic (2011).

Secondly, Smith et al. (2003) compared the standard CDM halo model to CDM simulations of large scale structure formation and developed an analytical fit to the non-linear corrections of the matter power spectrum, known as HALOFIT. We apply these corrections to a linear matter power suppressed by the Viel et al. (2005) WDM transfer function (see equation 1).

We show the results of these comparisons in Figure 7. As before, we plot the percent differences between the WDM and CDM matter power spectra obtained from our simulations of WDM only. We show this for particle masses of m_{WDM}=1 keV (left panels) and m_{WDM}=0.5 keV (right panels) at redshifts $z = 1$ (top row) and $z = 0.5$ (bottom row). We find that the WDM halo model is closest to simulations at redshift $z = 1$ for m_{WDM}=1 keV, but that it over-estimates the suppression effect at redshift $z = 0.5$ for m_{WDM}=0.5 keV WDM by about 5 percent on scales $k > 1$ $h\,\mathrm{Mpc}^{-1}$. On scales $k < 1$ $h\,\mathrm{Mpc}^{-1}$however, the HALOFIT non-linear correction describes the simulations better than the halo model, even though on smaller scales it severely underestimates the suppression effect, which becomes worse at lower redshifts. A further small modification of the WDM halo model will improve its correspondence to the simulations and allow to use it at small scales.

We additionally consider these models of non-linear WDM structure to calculate the weak lensing power spectra in order to explore the significance of using the correct model. We again plot percentage differences between WDM and CDM weak lensing power spectra in Figure 8. We show only curves representing the cross correlation power spectrum of redshift bins at $z = 1$ and $z = 1.6$ for consistency with Figure 6. We again examine WDM models with particle masses of m_{WDM}=1 keV (left panel) and m_{WDM}=0.5 keV (right panel). We also calculate the weak lensing power spectra without non-linear corrections to the matter power spectrum and note that this severely over-estimates the effect of WDM suppression. In the lensing calculation, the HALOFIT non-linear corrections applied to the WDM sup-

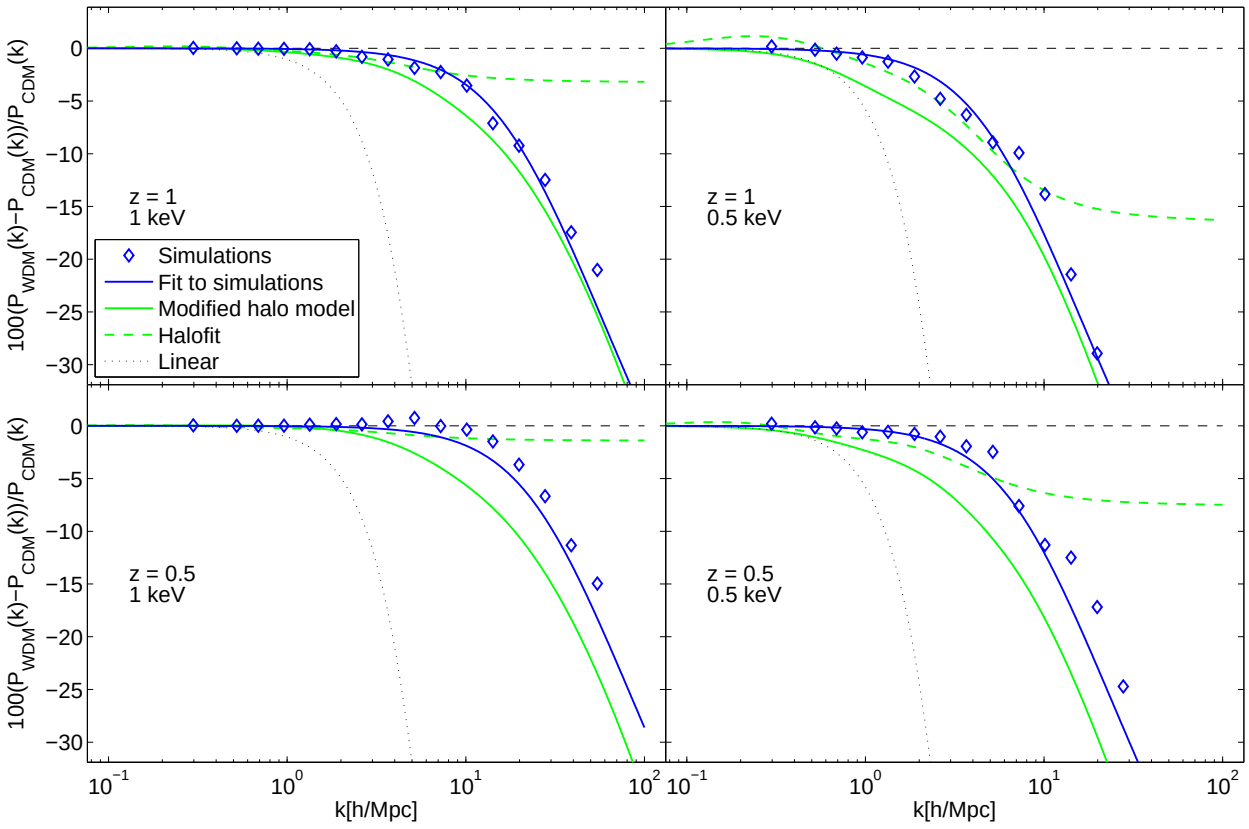

Figure 7. The comparison of different non-linear models at redshifts $z = 1.0$ (top panels) and $z = 0.5$ (bottom panels) for WDM particles with masses 1 keV (left panels) and 0.5 keV (right panels). The blue diamonds represent the fractional differences calculated from DM-only simulations from previous plots with the fiducial values for σ_8. The blue solid lines are the corresponding analytical fits from equation 2. The green solid lines are calculated using the modified halo model, whereas the green dashed line is the standard HALOFIT. The dotted line is the effect as seen in the linear matter power spectrum.

pressed linear matter power spectrum seem to perform better in describing the results of our WDM simulations than than the WDM halo model. This is most likely due to the fact that the range of wavenumbers that are better described by the HALOFIT corrections, namely $k < 1h\,\mathrm{Mpc}^{-1}$ are significantly more relevant to the weak lensing power spectrum than the smaller scales where HALOFIT deviates from the simulation results. Using the linear WDM suppression transfer function as recently done in Semboloni et al. (2011) can significantly overestimates the effect of WDM on the weak lensing power at $l > 1000$ as compared to the CDM case.

6 CONCLUSIONS

By using a large set of N-body and hydrodynamic simulations we have explored the non-linear evolution of the total matter power. The focus of the present work is on small scales and relatively low redshifts where non-linear effects are important and need to be properly modelled with simulations. We checked for numerical convergence and box-sizes/resolution effects in the range $k = 1 - 10\,h\,\mathrm{Mpc}^{-1}$. We explored how different masses of a warm dark matter candidate affect the non-linear suppression as compared to a corresponding ΛCDM model that shares the same parameters and astrophysical inputs. Our findings can be summarized as follows:

- Cosmological volumes of linear size $25h^{-1}$ comoving Mpc are sufficient to sample the WDM suppression for $\mathrm{m_{WDM}} \geqslant 1$ keV with great accuracy.
- The non-linear suppression induced by WDM is strongly redshift dependent: however, by $z = 0$, up to $k = 10\,h\,\mathrm{Mpc}^{-1}$, there are virtually no differences between ΛCDM and WDM models with $\mathrm{m_{WDM}} \geqslant 1$ keV.
- At higher redshifts differences are larger, being closer to the linear suppression, and at $z \sim 1$ there are differences of the order of a few percent between the non-linear WDM and ΛCDM power spectra.
- Baryonic physics and in particular radiative processes for the gas component, the star formation criterion and galactic feedback are likely to affect the matter power at the 2-3 % level in the range $k = 1 - 10\,h\,\mathrm{Mpc}^{-1}$.
- We investigate how a change in Ω_m, H_0 and σ_8 impact on the non-linear power and in particular on the WDM suppression when values different from our reference choice are used and found small difference at the $\pm$ 2% level at the scales considered here: thus the WDM cutoff has a distinc-

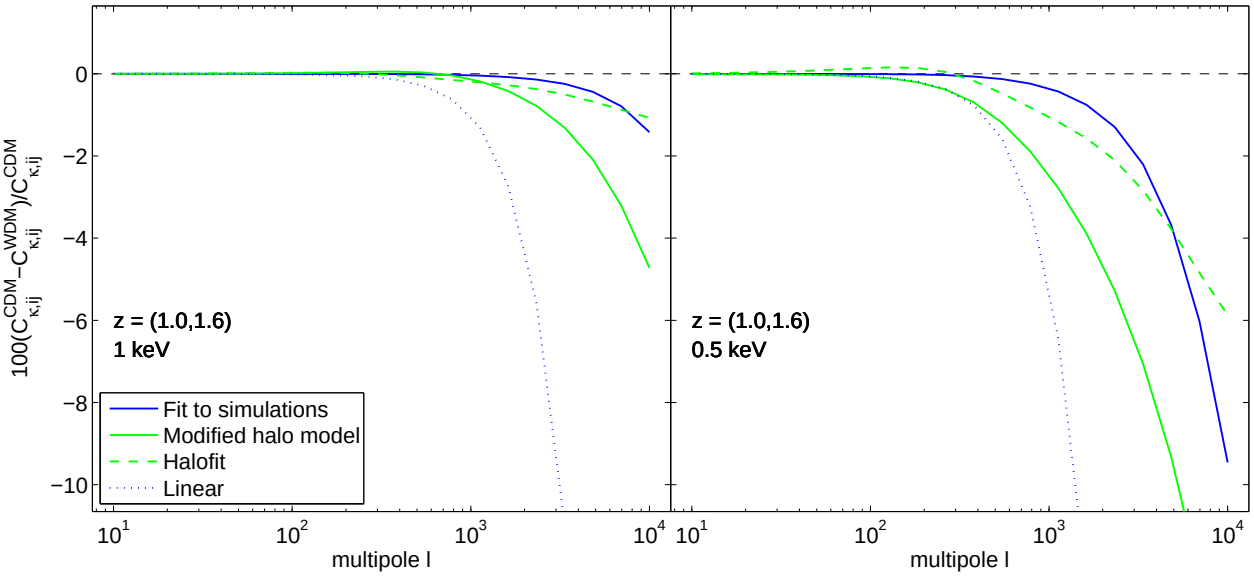

Figure 8. The comparison of the impact of using different models of non-linear power spectra from figure 7 on the weak lensing power spectrum. As above, the blue line is the fractional difference in percent between weak lensing power spectra calculated using the fitting function found in this work (2). The green solid line is the weak lensing power spectrum calculated using the halo model modified for WDM. The dashed green line is the same using standard HALOFIT. The dotted line is calculated by omitting all non-linear corrections. It is evident that excluding such corrections causes a significant overestimation of the WDM effect. All the lines in this plot are calculated from cross power spectra of the 5th and 8th tomographic bins (corresponding to $z = 1.6$ and $z = 1$, respectively) for WDM particle masses of m_{WDM}=1 keV (left panel) and m_{WDM}=0.5 keV (right panel).

tive feature which is not degenerate with other cosmological parameters also at a non-linear level.

- We provide a useful fit to the non-linear WDM induced suppression in terms of a redshift-dependent transfer function; this fitting formula should agree to the actual measured power at the 2% level at $z < 3$ and for masses above 0.5 keV.

- Reaching a higher accuracy (percent level) in terms of WDM non-linear power would require a much more careful analysis of astrophysical aspects related to the baryonic component.

- We find that future weak lensing surveys will most likely be powerful enough to rule out WDM masses smaller than 1 keV, which is consistent with previous results of Markovic et al. (2011) and Smith & Markovic (2011). Ruling out models for masses larger than 1 keV would still be possible by using the cross-correlation signal between different redshift bins.

- Non-linear corrections to the matter power spectrum in the WDM scenario obtained from HALOFIT correspond better to the results of the WDM only simulation at scales $k < 1$ $h\,\mathrm{Mpc}^{-1}$, but on smaller scales the WDM halo model of Smith & Markovic (2011) performs better and suggests that a further modification to the halo model might be needed, especially for weak lensing power spectrum calculations.

We believe that future efforts aiming at measuring the coldness of cold dark matter should investigate the non-linear matter power in the range $z = 0 - 5$ either using weak lensing observables or the small scale clustering of galaxies. These constraints can be particularly useful since they are complementary to those that can be obtained from high redshift Lyman-α forest data (e.g. BOSS/SDSS-III survey) or galactic and sub-galactic observables in the local universe.

ACKNOWLEDGMENTS.

We are grateful to Robert Smith for providing tables to calculate the halo model power spectrum. Numerical computations were performed at the High Performance Computer Cluster Darwin (HPCF) in Cambridge (UK) and at the RZG computing center in Garching. We acknowledge support from an ASI/AAE grant, ASI contracts Euclid-IC (I/031/10/0), INFN PD51, PRIN MIUR, PRIN INAF 2009, ERC-StG "cosmoIGM". Post-processing od the simulations has also been carried at CINECA (Italy) and COSMOS Supercomputer in Cambridge (UK). KM acknowledges support from the International Max-Planck Research School.

REFERENCES

Abazajian K., 2006, Phys. Rev. D, 73, 063513
Abbott T., et al., 2005, arXiv:astro-ph/0510346
Baldi M., 2011, MNRAS, 414, 116
Bartelmann M., Schneider P., 2001, Physics Reports, 340, 291
Bode P., Ostriker J. P., Turok N., 2001, ApJ, 556, 93
Bolton J. S., Haehnelt M. G., Viel M., Springel V., 2005, MNRAS, 357, 1178
Boyarsky A., Lesgourgues J., Ruchayskiy O., Viel M., 2009a, JCAP, 5, 12

Boyarsky A., Lesgourgues J., Ruchayskiy O., Viel M., 2009b, Physical Review Letters, 102, 201304
Brandbyge J., Hannestad S., Haugbølle T., Thomsen B., 2008, JCAP, 8, 20
Casarini L., La Vacca G., Amendola L., Bonometto S. A., Macciò A. V., 2011, JCAP, 3, 26
Coil A. L., Newman J. A., Croton D., Cooper M. C., Davis M., Faber S. M., Gerke B. F., Koo D. C., Padmanabhan N., Wechsler R. H., Weiner B. J., 2008, ApJ, 672, 153
Colín P., Avila-Reese V., Valenzuela O., 2000, ApJ, 542, 622
Colín P., Valenzuela O., Avila-Reese V., 2008, ApJ, 673, 203
Colombi S., Jaffe A., Novikov D., Pichon C., 2009, MNRAS, 393, 511
Cooray A., Sheth R., 2002, Physics Reports, 372, 1
Dodelson S., Widrow L. M., 1994, Phys. Rev. Lett., 72, 17
Gao L., Theuns T., 2007, Science, 317, 1527
Guillet T., Teyssier R., Colombi S., 2010, MNRAS, 405, 525
Hansen S. H., Lesgourgues J., Pastor S., Silk J., 2002, MNRAS, 333, 544
Hill G. J., et al., 2008, ASP Conf. Ser., 399, 115
Hu W., 1999, The Astrophysical Journal, 522, L21
Ivezic Z., et al., 2008, arXiv:0805.2366
Jenkins A., Frenk C. S., Pearce F. R., Thomas P. A., Colberg J. M., White S. D. M., Couchman H. M. P., Peacock J. A., Efstathiou G., Nelson A. H., 1998, ApJ, 499, 20
Kaiser N., et al., 2002, Proc. SPIE Int. Soc. Opt. Eng., 4836, 154
Katz N., Weinberg D. H., Hernquist L., 1996, ApJS, 105, 19
Knebe A., Arnold B., Power C., Gibson B. K., 2008, MNRAS, 386, 1029
Komatsu E., et al., 2011, ApJS, 192, 18
Lesgourgues J., Tram T., 2011, ArXiv e-prints
Lewis A., Challinor A., Lasenby A., 2000, Astrophys. J., 538, 473
Lovell M., Eke V., Frenk C., Gao L., Jenkins A., Theuns T., Wang J., Boyarsky A., Ruchayskiy O., 2011, ArXiv e-prints
Ma C.-P., 1996, Astrophysical Journal v.471, 471, 13
Macciò A. V., Fontanot F., 2010, MNRAS, 404, L16
Markovic K., Bridle S., Slosar A., Weller J., 2011, JCAP, 1, 22
Massey R., Rhodes J., Leauthaud A., Capak P., Ellis R., Koekemoer A., Refregier A., Scoville N., Taylor J. E., Albert J., Berge J., Heymans C., Johnston D., Kneib J.-P., Mellier Y., Mobasher B., Semboloni E., Shopbell P., Tasca L., Waerbeke L. V., 2007, arXiv, astro-ph
Navarro J. F., Frenk C. S., White S. D. M., 1995, arXiv, astro-ph
Polisensky E., Ricotti M., 2011, Phys. Rev. D, 83, 043506
Press W. H., Schechter P., 1974, ApJ, 187, 425
Refregier A., et al., 2010, arXiv:1001.0061
Rudd D. H., Zentner A. R., Kravtsov A. V., 2008, ApJ, 672, 19
Seljak U., 2000, Monthly Notices of the Royal Astronomical Society, 318, 203
Seljak U., Makarov A., McDonald P., Trac H., 2006, Physical Review Letters, 97, 191303
Seljak U. e. a., 2005, Phys. Rev. D, 71, 103515
Semboloni E., Hoekstra H., Schaye J., van Daalen M. P., McCarthy I. G., 2011, ArXiv e-prints
Smith R. E., Markovic K., 2011, ArXiv e-prints
Smith R. E., Peacock J. A., Jenkins A., White S. D. M., Frenk C. S., Pearce F. R., Thomas P. A., Efstathiou G., Couchman H. M. P., 2003, MNRAS, 341, 1311
Springel V., 2005, MNRAS, 364, 1105
Springel V., Hernquist L., 2003, MNRAS, 339, 289
Springel V., Hernquist L., 2003, Mon. Not. Roy. Astron. Soc., 339, 312
Strigari L. E., Bullock J. S., Kaplinghat M., Kravtsov A. V., Gnedin O. Y., Abazajian K., Klypin A. A., 2006, ApJ, 652, 306
Takada M., Jain B., 2004, Monthly Notices of the Royal Astronomical Society, 348, 897
Tikhonov A. V., Gottlöber S., Yepes G., Hoffman Y., 2009, MNRAS, 399, 1611
Trujillo-Gomez S., Klypin A., Primack J., Romanowsky A. J., 2010, ArXiv e-prints
van Daalen M. P., Schaye J., Booth C. M., Dalla Vecchia C., 2011, ArXiv e-prints
Viel M., Haehnelt M. G., Lewis A., 2006, MNRAS, 370, L51
Viel M., Haehnelt M. G., Springel V., 2004, MNRAS, 354, 684
Viel M., Haehnelt M. G., Springel V., 2010, JCAP, 6, 15
Viel M., Lesgourgues J., Haehnelt M. G., Matarrese S., Riotto A., 2005, Phys. Rev. D, 71, 063534
Viel M., Lesgourgues J., Haehnelt M. G., Matarrese S., Riotto A., 2006, Physical Review Letters, 97, 071301
Wang J., White S. D. M., 2007, MNRAS, 380, 93
Zavala J., Jing Y. P., Faltenbacher A., Yepes G., Hoffman Y., Gottlöber S., Catinella B., 2009, ApJ, 700, 1779